Available online at www.CivileJournal.org

Civil Engineering Journal

(E-ISSN: 2476-3055; ISSN: 2676-6957)

Vol. 12, No. 04, April, 2026

Evaluating Signal Processing Methods for Instantaneous Frequency Analysis in Time-Varying Mass Structures

Chinnapat Buachart [1], Chayanon Hansapinyo [1*], Teewara Suwan [1], Vanissorn Vimonsatit [2], Phung Tu [3], Worathep Sae-Long [4], Suchart Limkatanyu [5], Panatchai Chetchotisak [6]

[1] *Department of Civil Engineering, Faculty of Engineering, Chiang Mai University, Chiang Mai 50200, Thailand.*

[2] *School of Engineering, Faculty of Science and Engineering, Macquarie University, Sydney, NSW 2019, Australia.*

[3] *Flow Without Quake, Perth, Western Australia 6000, Australia.*

[4] *Civil Engineering Program, School of Engineering, University of Phayao, Phayao 56000, Thailand.*

[5] *Department of Civil and Environmental Engineering, Faculty of Engineering, Prince of Songkla University, Songkhla 90112, Thailand.*

[6] *Department of Civil Engineering, Rajamangala University of Technology Isan, Khon Kaen Campus, Khon Kaen 40000, Thailand.*

Received 29 September 2025; Revised 18 March 2026; Accepted 22 March 2026; Published 01 April 2026

Abstract

Time-varying mass (TVM) structures exhibit complex dynamic phenomena but remain insufficiently investigated, particularly in the frequency domain. For example, granular discharge in silos generates vibrations due to rapid mass reduction, leading to nonlinear and non-stationary responses. This study aims to evaluate the capability of three common signal processing algorithms–Empirical Mode Decomposition (EMD), Variational Mode Decomposition (VMD), and Empirical Wavelet Transform (EWT)–for analysing instantaneous frequency variations in TVM structures. The signals are first decomposed into mono-component modes and subsequently analyzed using the Hilbert transform to extract instantaneous frequency. The investigation is conducted in two stages: (i) numerical validation using an artificial nonlinear signal and a time-varying parameter SDOF system with known frequency histories, and (ii) application to experimental acceleration data obtained from sand discharge in a polycarbonate silo under noisy conditions. The findings show that EMD provides the most accurate frequency estimation for clean signals, whereas VMD and EWT demonstrate improved stability for experimental data with significant noise. The study provides a systematic comparison of decomposition–based instantaneous frequency methods in TVM structures and highlights the importance of appropriate method selection for safer and more reliable frequency-domain structural design.

Keywords: Time-Varying Mass Structure; Frequency Domain; Fourier Transform; Variational Mode Decomposition; Empirical Mode Decomposition; Empirical Wavelet Transform.

1. Introduction

Under service loading, the physical properties of most civil engineering structures–such as mass, damping, and stiffness–do not vary significantly over time. These structures are therefore generally classified as time-invariant systems. The design of such structures subjected to vibration is typically based on their initial dynamic properties. However, under extreme loads, such as strong earthquakes, structural damage may lead to reduced stiffness and increased damping [1, 2]. Consequently, seismic design guidelines adopt response spectra that incorporate predefined levels of structural damping. Similarly, aging and corrosion cause physical changes in structures, although these changes occur gradually throughout their service life [3-5].

* Corresponding author: chayanon@eng.cmu.ac.th

https://doi.org/10.28991/CEJ-2026-012-04-05

© 2026 by the authors. Licensee C.E.J, Tehran, Iran. This article is an open access article distributed under the terms and conditions of the Creative Commons Attribution (CC-BY) license (http://creativecommons.org/licenses/by/4.0/).

In contrast, certain civil engineering structures experience significant mass variations within a relatively short operational period. A typical example is a bulk solid container undergoing discharge. These structures are classified as time-varying mass (TVM) systems [6], characterized by rapid changes in mass, damping, and stiffness over the loading period. A distinctive aspect of TVM structures lies in the multidirectional interaction between the discharging material and the container walls, where the mechanical properties of the granular material also influence the overall dynamic responses. Although design codes such as Eurocode 1 (EN 1991-4) [7], AS 3774 [8], and ACI 313 [9] provided guidance for static and quasi-static silo loading, they do not explicitly address the dynamic effects induced by rapid mass variation during discharge.

The general process for analyzing a TVM structure resembles that of a conventional time-invariant structure, however, it requires explicit consideration of the rate of mass change and the bidirectional interaction between the container and the bulk material. Figure 1 outlines the typical analysis procedure for a TVM system. For bulk solid containers, elastic deformations prior to discharge are influenced by material properties such as density, moisture content, cohesion, particle size distribution, and wall friction. Once discharge begins, both static and dynamic equilibrium conditions must be satisfied throughout the mass loss cycle. The problem can be solved in either the time domain or the frequency domain [10]. The time-domain approach is more commonly used but requires checking mass variation at each time step. Conversely, the frequency-domain method has the potential to provide clearer insights into structural behavior, although research in this area remains limited. Advancing the frequency-domain approach requires a better understanding of the signals generated during discharge and their relationship to structural response.

Previous studies have reported that silo discharge generates dynamic forces with non-repetitive amplitudes and varying frequency content [11, 12]. Experimental investigations have demonstrated that vibration characteristics strongly depend on structural stiffness, discharge rate, particle properties, and moisture content [13-18]. These observations raise a critical design question: what frequency ranges and amplitudes should engineers consider to ensure structural safety and performance in TVM systems? Although the traditional Fourier Transform (FT) is widely used, it has inherent limitations in capturing the nonlinear and non-stationary characteristics of signals generated by granular discharge.

Advanced signal processing techniques have been widely adopted in various engineering disciplines, including mechanical systems with moving masses, rotating machinery fault diagnosis, vibration control of manipulators, and structural health monitoring of aerospace and automotive components. Methods such as the enhanced Empirical Wavelet Transform (EWT) combined with the Synchro Extracting Transform (SET), as well as the Choi–Williams distribution, have demonstrated effectiveness in identifying instantaneous dominant components and analysing energy distributions in non-stationary signals [19, 20]. However, research on applying advanced signal processing methods to TVM silo structures remains limited. Tu et al [21] employed Hilbert transform-based analysis and Variational Mode Decomposition (VMD) to extract dominant frequency components from silo vibration signals, enabling non-disruptive structural integrity assessment. Hernández-Juárez et al. [22] analyzed acoustic emissions during granular discharge; however, it did not identify the corresponding structural response, and only the conventional Fast Fourier Transform (FFT) was applied.

Despite the diversity and maturity of these techniques, their application to time-varying mass civil engineering structures—particularly silos undergoing granular discharge—remains comparatively limited. Most existing silo studies focus on load characterization or dominant frequency identification, rather than systematically evaluating instantaneous frequency extraction methods capable of capturing continuously evolving dynamic behavior. Furthermore, the relative performance of these methods under different signal conditions (noise-free numerical data versus noisy experimental measurements) has not been clearly established. Therefore, a clear research gap exists: although TVM systems inherently exhibit time-varying and nonlinear frequency characteristics, there is insufficient comparative assessment of advanced decomposition techniques for accurately capturing instantaneous frequency evolution in such structures.

To address this gap, the present study evaluates the performance of Empirical Mode Decomposition (EMD), Variational Mode Decomposition (VMD), and Empirical Wavelet Transform (EWT) in extracting instantaneous frequency variations from TVM systems. The investigation is conducted in two stages. First, artificial nonlinear signals and a single-degree-of-freedom (SDOF) system with time-varying parameters are analyzed to validate the accuracy of each method against known theoretical frequency histories. Second, experimental acceleration data obtained from a discharging silo are processed to evaluate robustness under realistic noisy conditions.

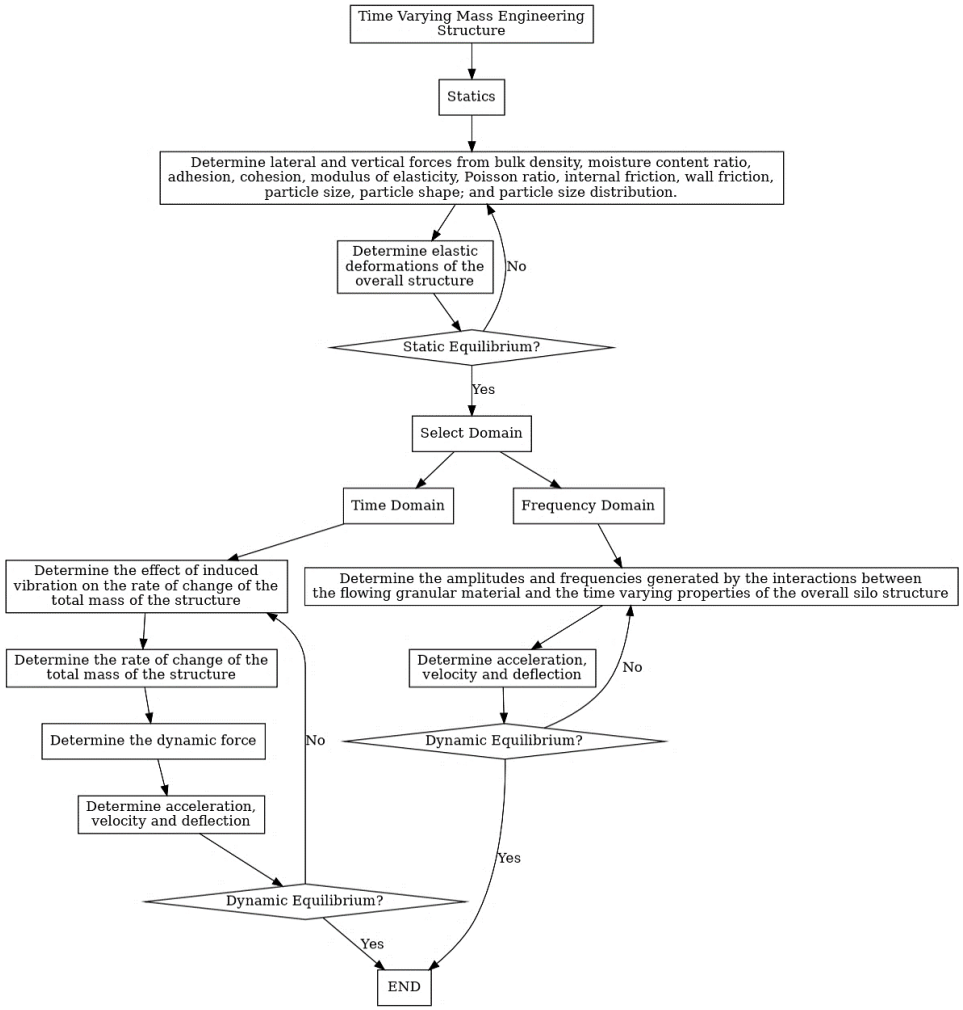

Figure 1. Analysis procedure for a Time-Varying Mass (TVM) engineering structure

The primary contributions of this work are threefold: (i) providing a systematic comparison of EMD, VMD, and EWT for TVM structural applications; (ii) clarifying their strengths and limitations under varying noise conditions; and (iii) supporting the development of a frequency-domain analysis framework for the safer and more reliable design of time-varying mass engineering structures. Figure 2 summarizes the overall research methodology.

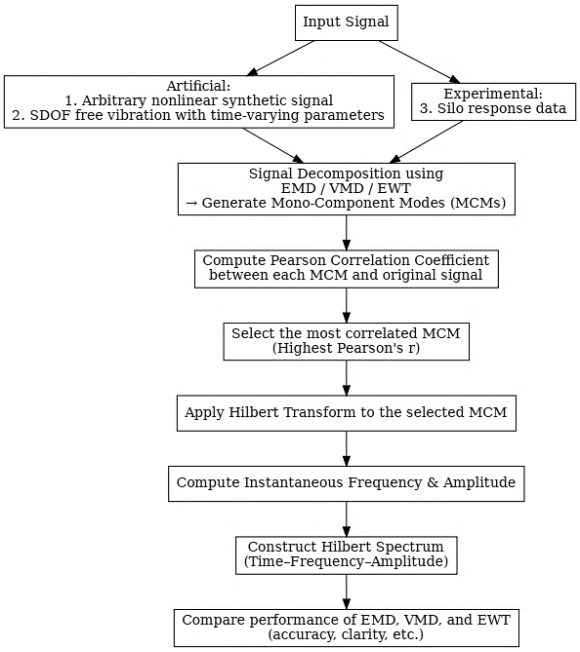

Figure 2. Overview of the present study

2. Research Methodology

The study of frequency content in data collected from silos remains limited, resulting in a lack of reference frequency data for benchmarking the performance of various signal processing methods. To address this gap, an artificial nonlinear and non-stationary signal with known frequency components is generated. This synthetic signal serves as a benchmark for evaluating the effectiveness of different signal processing methods, including the Fourier Transform (FT), Empirical Mode Decomposition (EMD), Variational Mode Decomposition (VMD), and Empirical Wavelet Transform (EWT). The artificial signal is designed to simulate the frequency-varying behavior commonly observed in time-varying mass (TVM) systems, such as those encountered during silo discharge processes. These methods are then applied to analyze experimentally measured signals obtained from a silo during discharge.

2.1. Determination of Instantaneous Frequency

To determine the instantaneous frequency, the generated signal is analyzed in the time domain and decomposed into multiple mono-component signals [23]. This study employs various decomposition techniques, including Empirical Mode Decomposition (EMD), Variational Mode Decomposition (VMD), and Empirical Wavelet Transform (EWT). The time-varying instantaneous frequencies are then derived by applying the Hilbert transform (HT) to the mono-component signal that exhibits the highest correlation with the original signal. This selection criterion is adopted because cross-correlation directly quantifies waveform similarity and temporal coherence, which are essential for stable instantaneous frequency estimation using the Hilbert transform. Unlike energy-based selection methods, correlation ensures that the extracted component preserves the dominant oscillatory behavior and phase structure governing the structural response.

The decomposition of the original signal into multiple mono-components can be described as:

$$x(t) = \sum_{k=1}^{N} u_k(t) + r_N(t) \tag{1}$$

where, $x(t)$ is the original nonlinear signal, $u_k(t)$ is the k-th mono-component signal, N is the total number of modes, and $r_N(t)$ is the residual.

Thus, the original signal $x(t)$ is decomposed into a set of narrowband mono-components suitable for further analysis. Implementation details of EMD, VMD and EWT used in the decomposition process can be found in [24-26]. These decomposed components are assumed to possess well-defined instantaneous frequencies, enabling consistent application of the Hilbert transform.

To obtain the time-varying instantaneous frequency of each mono-component signal, the Hilbert transform (HT) of the k-th mono-component $u_k(t)$ is defined as [23]:

$$\tilde{u}_k(t) = \frac{P}{\pi}\int_{-\infty}^{\infty} \frac{u_k(\tau)}{t-\tau} d\tau \tag{2}$$

where $\tilde{u}_k(t)$ is the Hilbert transform of $u_k(t)$, P indicates the Cauchy principal value, and τ is the integration variable. The analytic signal $(z_k(t))$ corresponding to $u_k(t)$ is then expressed as:

$$z_k(t) = u_k(t) + j\tilde{u}_k(t) = A_k(t)e^{j\theta_k(t)} \tag{3}$$

where, j is the imaginary unit (i.e. $j^2 = -1$). The instantaneous amplitude $A_k(t)$ and phase angle $\theta_k(t)$ are respectively defined as:

$$A_k(t) = |z_k(t)| = \sqrt{u_k^2(t) + \tilde{u}_k^2(t)} \tag{4}$$

$$\theta_k(t) = \arctan(\tilde{u}_k(t)/u_k(t)) \tag{5}$$

The instantaneous frequency of the k-th mono-component $(f_k(t))$ is then obtained by differentiating the phase:

$$f_k(t) = \frac{1}{2\pi}\left(\frac{d\theta_k}{dt}\right) \tag{6}$$

This method provides a comprehensive time-frequency analysis for extracting instantaneous frequencies from time-varying signals. In addition to analysing the instantaneous frequency of the k-th mono-component mode as defined in Equation 6, an overall instantaneous frequency (IF) estimate of the signal x(t) is calculated as a weighted summation of the individual instantaneous frequencies [27]:

$$IF\big(x(t)\big) = \frac{\sum_{k=1}^{N} A_k^2(t) f_k(t)}{\sum_{k=1}^{N} A_k^2(t)} \tag{7}$$

where, $A_k(t)$ is the instantaneous amplitude of the analytic signal of the k-th mono-component mode, and N is the total number of modes.

The weighted-average instantaneous frequency defined in Equation 7 may be interpreted as an effective time-dependent modal frequency of the structure. By weighting each component's instantaneous frequency by its amplitude contribution, this measure captures the dominant dynamic behavior governing the structural response. In silo discharge scenarios, this combined frequency reflects stiffness evolution and mass redistribution effects, and may therefore be associated with potential resonance conditions when approaching structural natural frequencies.

2.2. Cross-Correlation Coefficient

The *k*-th mono-component signal $u_k(t)$, as defined in Equation 1, should maintain a meaningful relationship with the original signal. To quantify this relationship, the cross-correlation coefficient (r_k) between the original signal $x(t)$ and each *k*-th mono-component signal $u_k(t)$ is computed as follows [28]:

$$r_k = \frac{\sum_{i=1}^{M}(u_k(t_i)-\bar{u}_k)(x(t_i)-\bar{x})}{\sqrt{\sum_{i=1}^{M}(u_k(t_i)-\bar{u}_k)^2 \sum_{i=1}^{M}(x_k(t_i)-\bar{x}_k)^2}} \quad (8)$$

where $\bar{u}_k$ is the mean of $u_k(t)$, $\bar{x}$ is the mean of $x(t)$, and M is the number of samples in the time series.

The value of the cross-correlation coefficient r_k ranges between –1 and 1. A value of $r_k = 0$ indicates that $u_k(t)$ has no significant correlation with $x(t)$, while $|r_k| = 1$ indicates perfect correlation. This metric is not intended to evaluate all decomposed modes equally, but rather to identify the most representative mode that best captures the essential characteristics of the original signal. In practice, only the mode with the highest correlation coefficient is selected for subsequent Hilbert transform analysis. This step ensures that spurious or weakly correlated modes—often containing noise or artifacts—are excluded, thereby improving the accuracy of the estimated instantaneous frequency.

2.3. Free vibration of Time-Varying Mass Single-Degree-of-Freedom (SDOF) System

Consider the Equation of motion for a Single-Degree-of-Freedom (SDOF) system with time-varying parameters under free vibration [29-31]:

$$\frac{d}{dt}(m(t)\dot{u}(t)) + D(t)\dot{u}(t) + k(t)u(t) = 0 \quad (9)$$

where, $u(t)$ and $\dot{u}(t)$ are respectively the displacement and velocity responses. $m(t)$ is the time-varying mass, $D(t)$ is the viscous damping coefficient, and $k(t)$ is the stiffness coefficient of the SDOF system. The dot notation represents differentiation with respect to time (t). By applying the product rule of differentiation, Equation 9 can be rearranged as:

$$m(t)\ddot{u}(t) + c(t)\dot{u}(t) + k(t)u(t) = 0 \quad (10)$$

where, $\ddot{u}(t)$ is the acceleration response, and $c(t)$ is the equivalent time-varying damping coefficient defined as $c(t) = dm/dt + D(t)$. After normalizing by the mass $m(t)$, the standard form of Equation 10 becomes:

$$\ddot{u}(t) + 2\xi(t)\omega_0(t)\dot{u}(t) + \omega_0^2(t)u(t) = 0 \quad (11)$$

where, $\omega_0(t)$ and $\xi(t)$ are the time-varying natural angular frequency and damping ratio, respectively.

Equation 11 is solved numerically using the fourth-order Runge–Kutta method, given the initial displacement $u(0)$ and velocity $\dot{u}(0)$. Notably, when the damping coefficient is defined as $c(t) = dm/dt$, the analytical solution of Equation 11 can be expressed in terms of Bessel's functions [31]. The instantaneous natural angular frequency ($\omega_0(t)$) and damping ratio ($\xi(t)$) are updated at each time step and can be determined as follows:

$$\omega_0(t) = \sqrt{\left(\frac{d\ln A(t)}{dt}\right)^2 + \left(\frac{d\theta(t)}{dt}\right)^2} \quad (12)$$

$$\xi(t) = -\frac{1}{\omega_0}\left(\frac{d\ln A(t)}{dt}\right) \quad (13)$$

where, $A(t)$ and $\theta(t)$ are the instantaneous amplitude and phase angle of the analytic signal of the SDOF response, defined in Equations 4 and 5.

To identify the time-varying natural frequency of the SDOF system described in Equation 11, the calculated response–whether displacement, velocity, or acceleration–is decomposed into multiple mono-component modes. The most correlated mono-component mode, determined by the highest cross–correlation coefficient (Equation 8), is transformed into an analytic signal using the Hilbert transform, as described in Equations 1–3. Subsequently, the amplitude, $A(t)$, phase angle $\theta(t)$, and instantaneous frequency $f(t)$ are obtained from Equations 4–6. Figure 2 shows the calculation steps for signal decomposition.

3. Numerical Examples and Application of Signal Processing Techniques

In this section, two test cases are presented to illustrate the performance of EMD, VMD and EWT. The first case involves an artificial nonlinear and non-stationary signal, and the second examines the vibration response of a single-degree-of-freedom (SDOF) system with time-varying parameters.

3.1. Artificial Signal

3.1.1. Signal Formulation

A nonlinear and non-stationary signal is characterized by irregular vibrations in both amplitude and frequency, which change over time in a non-uniform manner. Consider the artificial nonlinear signal $x(t)$, defined as:

$$x(t) = (1 + 0.5\sin(0.1\pi t)) \cdot \sin(2\pi(0.1t + 0.495t^2)) \quad (14)$$

Equation 14 represents a signal with a time-varying amplitude envelope ($A(t)$):

$$A(t) = 1 + 0.5\sin(0.1\pi t) \quad (15)$$

The instantaneous frequency ($f(t)$ in Hz), according to Equation 6, is given by:

$$f(t) = 0.1 + 0.99t \quad (16)$$

The signal is generated over a duration of T_d = 10 seconds with a sampling frequency of f_s = 30 Hz. Given that the maximum signal frequency is 10 Hz, the Nyquist frequency (15 Hz) exceeds the highest frequency component, thereby satisfying the Nyquist criterion and preventing aliasing. The artificial signal was constructed with a linear frequency increase from 0.1 to 10 Hz to provide a controlled benchmark for validating the decomposition methods. Although real silo discharge signals may exhibit nonlinear or intermittent frequency variations, the linear chirp allows direct assessment of method accuracy under known frequency evolution. Figure 3-a shows the generated artificial signal using Equation 14.

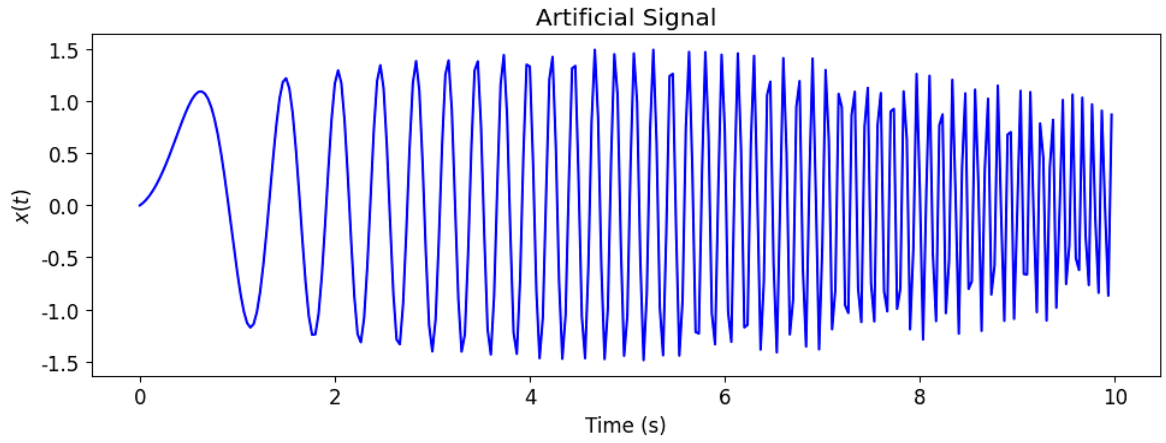

(a) Time history

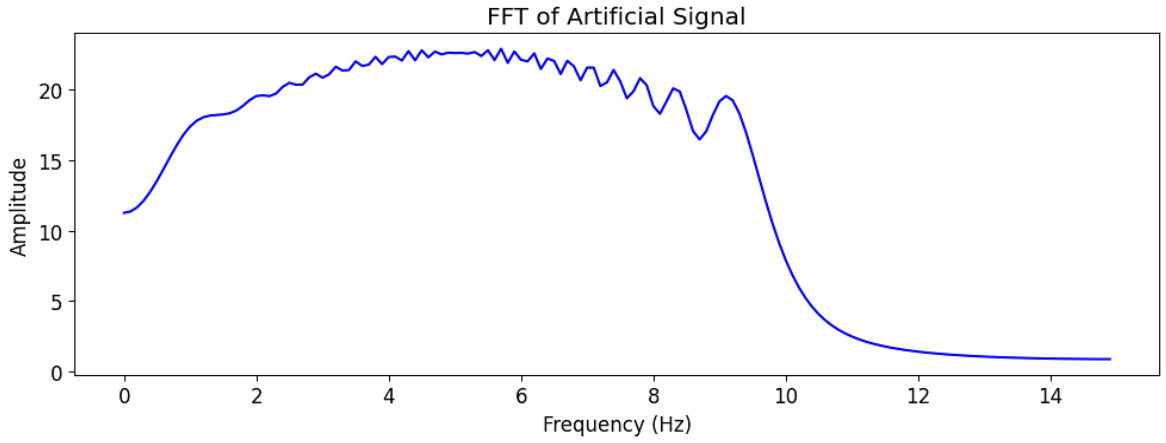

(b) Fourier spectrum

Figure 3. Artificial signal

3.1.2. Results of Analysis of the Artificial Signal

First, frequency analysis of the artificial signal is conducted using the Fourier Transform (FT). The corresponding Fourier spectrum is shown in Figure 3-b, indicating that the signal contains frequencies ranging from 0 to 15 Hz. This is a relatively low-frequency range, which is common in many structural vibrations. The amplitude increases from low frequencies and reaches a plateau between approximately 4–7 Hz, followed by a noticeable roll-off beyond approximately 9 Hz. This broadband spectral distribution reflects the frequency-modulated nature of the artificial signal shown in Figure 3-a, where the oscillation frequency increases continuously with time. Because the FT represents the signal in a global frequency sense, the increasing frequency content appears as a wide spectral band rather than a time-localized trajectory. Therefore, although the FT correctly captures the overall frequency range, it cannot describe the temporal evolution of frequency.

To observe instantaneous frequency variations over time, the signal is decomposed into four mono-component signals using the signal processing techniques (EMD, VMD, and EWT). The decomposed signals are shown in Figures 4-a, 5-a, and 6-a, respectively, along with their corresponding correlation values.

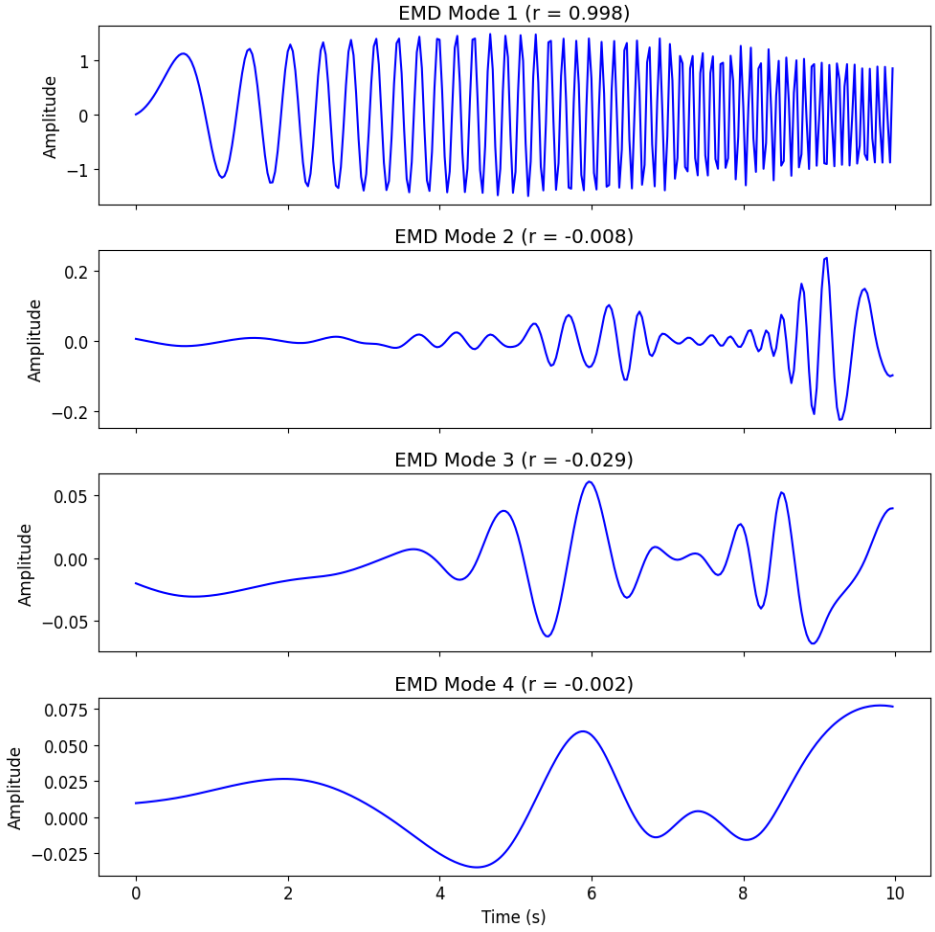

(a) First four mono-component modes of the artificial signal with corresponding cross-correlation factor

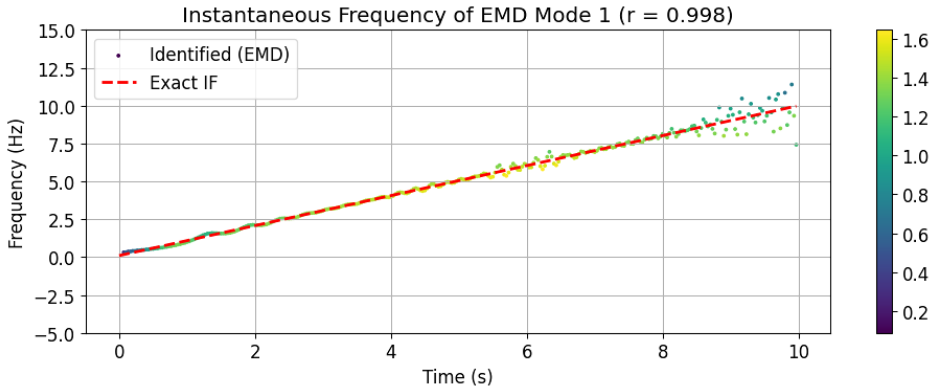

(b) Most correlated mono-component mode and the exact instantaneous frequencies (IFs)

Figure 4. Signal processing of the artificial signal using EMD

For EMD (Figure 4-a), Mode 1 shows a very high correlation coefficient (r = 0.998), indicating that nearly the entire frequency-modulated component is captured within a single intrinsic mode function (IMF). The remaining modes exhibit negligible correlation, implying limited mode mixing for this artificial signal. This confirms that EMD effectively isolates the dominant frequency-varying component under noise-free conditions. The corresponding instantaneous frequency shown in Figure 4-b closely follows the exact analytical frequency curve, demonstrating that EMD can accurately track continuous frequency evolution. Minor scatter observed at higher time values is likely attributable to numerical differentiation sensitivity during Hilbert transform processing, rather than decomposition errors.

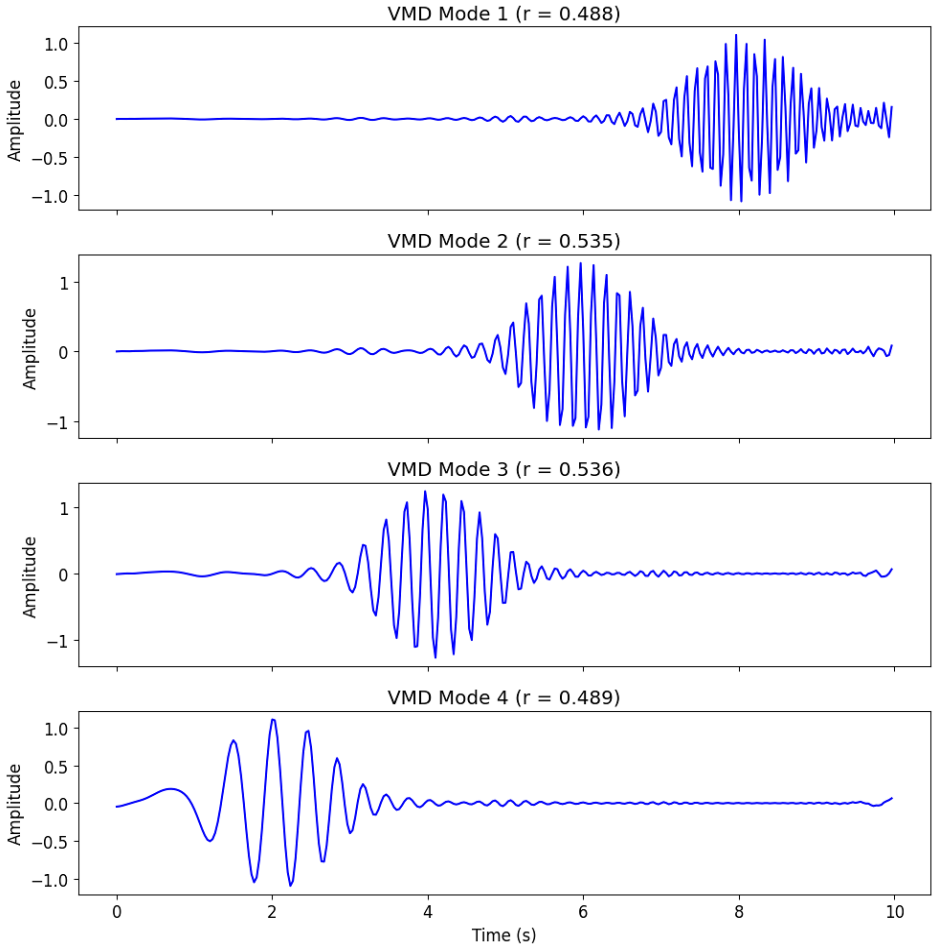

(a) First four mono-component modes of the artificial signal with corresponding cross-correlation factor

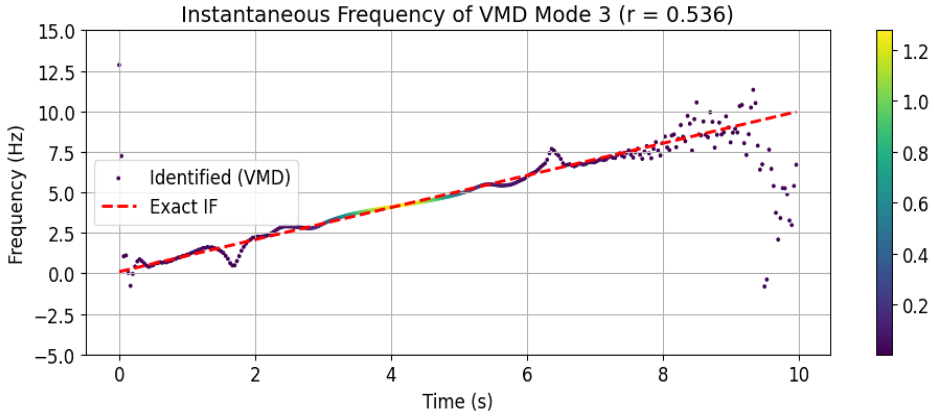

(b) Most correlated mono-component mode and the exact instantaneous frequencies (IFs

Figure 5. Signal processing of the artificial signal using VMD

In contrast, the VMD results in Figure 5-a show that the energy of the artificial signal is distributed among multiple modes, with moderate correlation coefficients (r ≈ 0.49–0.54). This indicates that the frequency-modulated component is not fully concentrated in a single mode but rather partitioned due to the bandwidth-constrained optimization

mechanism of VMD. As shown in Figure 5-b, although the extracted instantaneous frequency generally follows the increasing trend, noticeable fluctuations appear at later time stages when the frequency becomes higher. This behavior suggests that the fixed number of modes and bandwidth regularization may introduce frequency leakage or mode splitting when the instantaneous frequency changes rapidly.

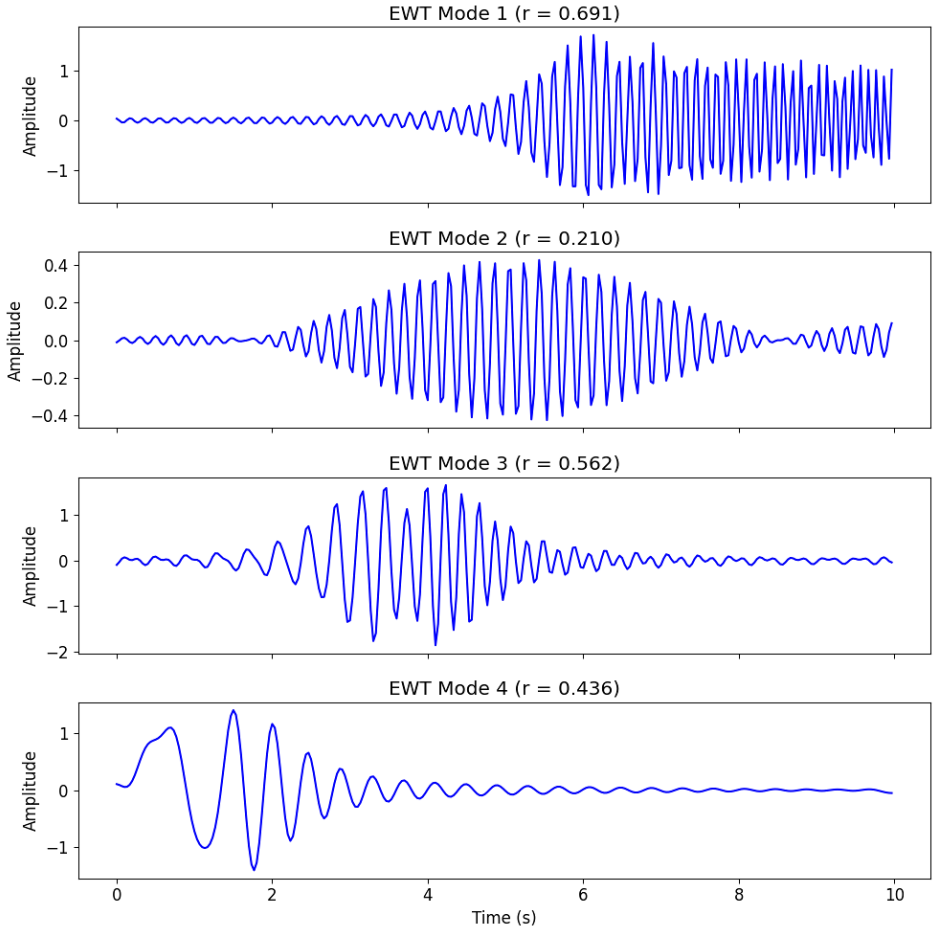

(a) First four mono-component modes of the artificial signal with corresponding cross-correlation factor

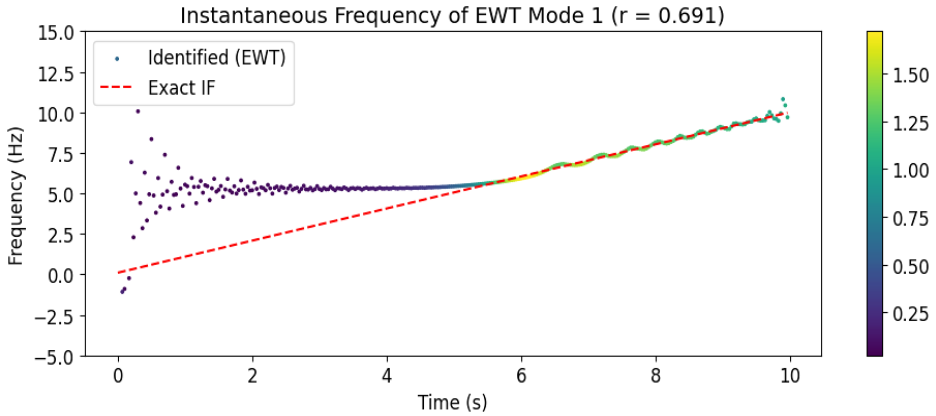

(b) Most correlated mono-component mode and the exact instantaneous frequencies (IFs)

Figure 6. Signal processing of the artificial signal using EWT

For EWT (Figure 6-a), Mode 1 shows the highest correlation (r = 0.691), while the remaining modes contain partial energy contributions. Since EWT relies on adaptive segmentation of the Fourier spectrum, the continuously increasing frequency of the artificial signal leads to spectral energy spreading across adjacent bands. Consequently, the dominant component is not completely isolated within a single mode. As shown in Figure 6-b, the instantaneous frequency estimation captures the overall increasing trend but exhibits larger deviations at early time instants. These deviations may be associated with imperfect spectral boundary detection during wavelet construction, especially when the signal contains low-frequency components transitioning rapidly.

Based on the Pearson correlation (r-value) and visual agreement with the exact frequency curve, the results indicate that EMD yields the lowest estimation error for the artificial signal, followed by EWT and VMD. Under ideal noise-free conditions, the fully adaptive nature of EMD allows precise tracking of frequency modulation. However, the smoother but slightly averaged behavior of VMD and the spectrum-dependent segmentation of EWT suggest that their performance may differ when applied to more complex or noisy signals, which will be examined in subsequent sections.

3.2. Response of Time-Varying Parameter SDOF Free Vibration System

3.2.1. Time-Varying Parameter SDOF System

The dynamic parameters of the SDOF free vibration system described in Equation 9 are defined as:

$$m(t) = e^t \text{ kg}$$
$$c(t) = e^t \text{ N} \cdot \frac{\text{s}}{\text{m}} \quad (17)$$
$$k(t) = 1600 \text{ N/m}$$

These time-varying mass ($m(t)$), damping ($c(t)$), and stiffness functions ($k(t)$) represent a simplified SDOF structural model with progressive mass redistribution during discharge. The model is intended to illustrate the effect of time-dependent parameters on frequency evolution and to provide a controlled framework for evaluating signal decomposition methods. The model is designed for methodological demonstration rather than direct replication of a specific measured silo system.

Thus, the normalized equation of motion (Equation 9) is rewritten as:

$$\ddot{u}(t) + \dot{u}(t) + 1600e^{-t}u(t) = 0 \quad (18)$$

The system mass is subjected to an initial displacement of $u(0)$ = 0.01 m and zero initial velocity $\dot{u}(0)$ = 0. In this study, Equation 18 is solved numerically using the fourth-order Runge-Kutta method with a time step of 0.01 s over a 4.0 s duration. The resulting acceleration response is then analyzed using EMD, VMD, and EWT signal processing techniques.

3.2.2. Results of the Free Vibration Analysis

The numerical solution of the SDOF response based on Equation 18 is shown in Figure 7. The exact displacement solution [31] is also plotted for the first 1.0 s (with a time step of 0.05 s) to verify the accuracy of the Runge–Kutta method. The close agreement between the numerical and exact solutions in the early stage confirms the correctness and stability of the time integration procedure.

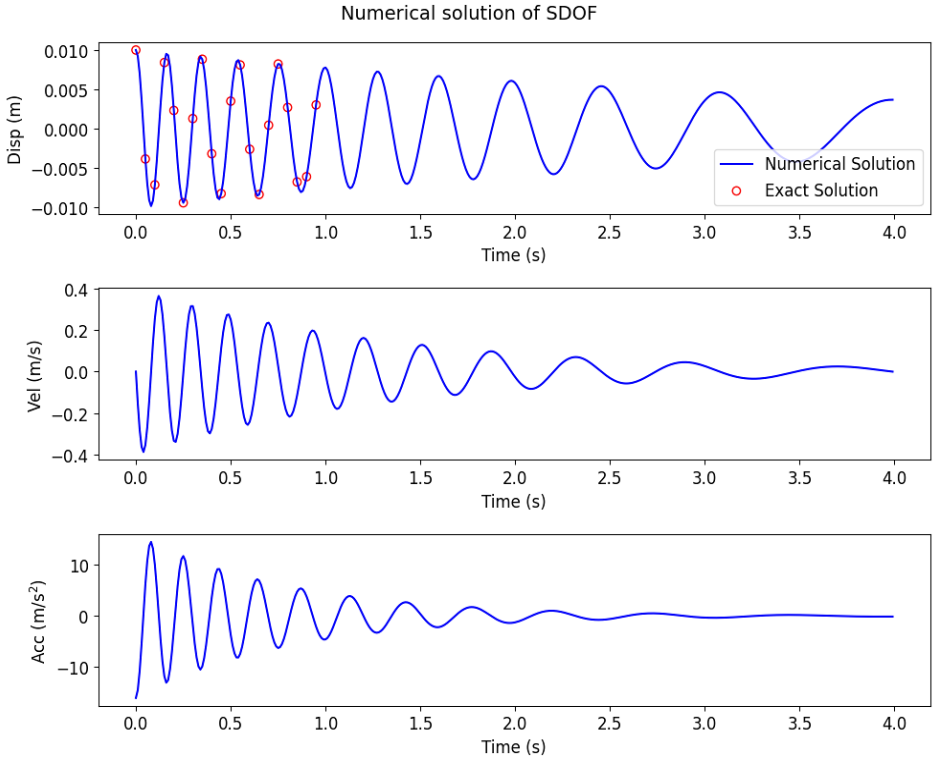

Figure 7. Vibration responses of the SDOF free vibration system with time-varying parameters

Figure 7 shows that the vibration amplitude gradually decays with time due to damping effects, while the oscillation period increases progressively. Physically, this behavior results from the time-varying system parameters, particularly the increase in effective mass (or reduction in stiffness-to-mass ratio, k/m), which reduces the natural frequency (ω_n) according to the classical relation $\omega_n = \sqrt{k/m}$. Therefore, the SDOF model represents a simplified yet physically meaningful benchmark for validating instantaneous frequency tracking methods.

The acceleration response from Figure 7 is treated as the measured signal $x(t)$ and decomposed using EMD, VMD, and EWT. The instantaneous phase angle $\theta(t)$ and amplitude $A(t)$ are obtained by applying the Hilbert transform to the most correlated mode. The identified time-varying natural frequency of SDOF system is then calculated from Equation 12.

Figures 8-a to 8-c present the most correlated mono-component mode obtained from EMD, VMD, and EWT, respectively, compared with the numerical solution. For EMD, the correlation coefficient reaches r = 1.000, indicating that the dominant oscillatory component of the SDOF response is almost entirely captured within a single intrinsic mode function. This confirms the strong adaptiveness of EMD for systems with a single smoothly varying frequency. For VMD (r = 0.896), the primary oscillation is well represented; however, the lower correlation suggests partial energy distribution among adjacent modes due to the imposed bandwidth constraints. This effect becomes more noticeable at later stages when the vibration amplitude decreases. The EWT result (r = 0.994) shows performance comparable to EMD. The dominant mode clearly represents the decaying oscillation, demonstrating effective spectral segmentation for this relatively clean signal.

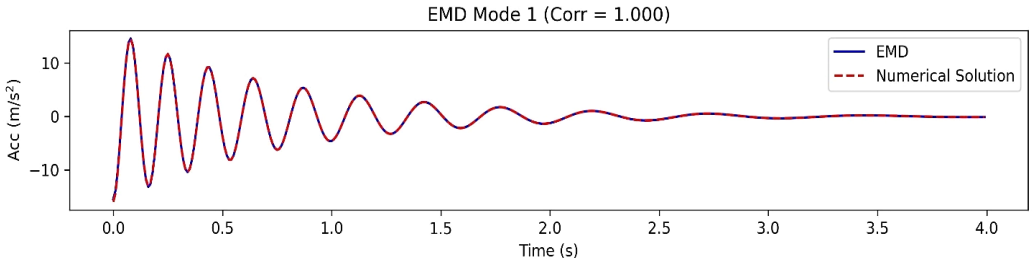

(a) EMD

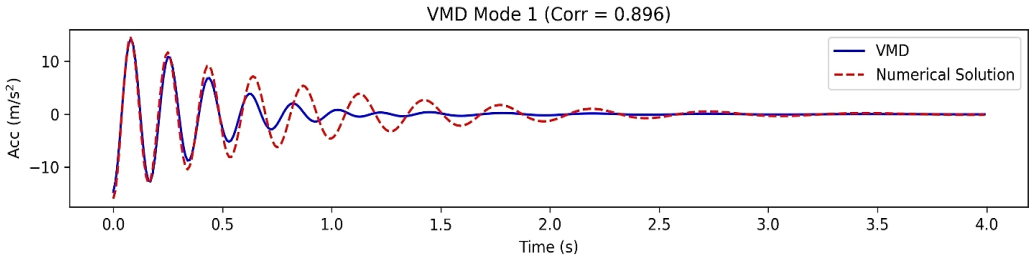

(b) VMD

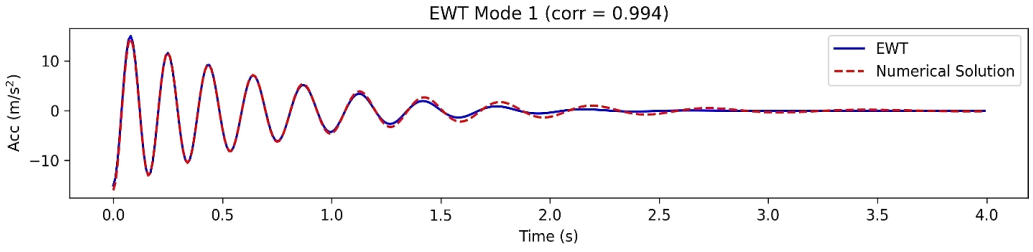

(c) EWT

Figure 8. Most correlated mono-component mode of the SDOF system

The identified natural frequency histories in Figures 9-a to 9-c are compared with the exact analytical solution. For EMD, the extracted frequency closely follows the exact decreasing trend, with minor deviations appearing at later times (t > 3 s) when the response amplitude becomes very small. Such deviations are expected, as Hilbert-based instantaneous frequency estimation becomes sensitive when signal energy is low. VMD captures the overall decreasing trend but shows stronger fluctuations in the mid-to-late stages, likely caused by mode splitting and reduced signal-to-noise ratio. EWT agrees well with the exact solution in the early and mid-stages, with small deviations at later times for similar amplitude-related reasons.

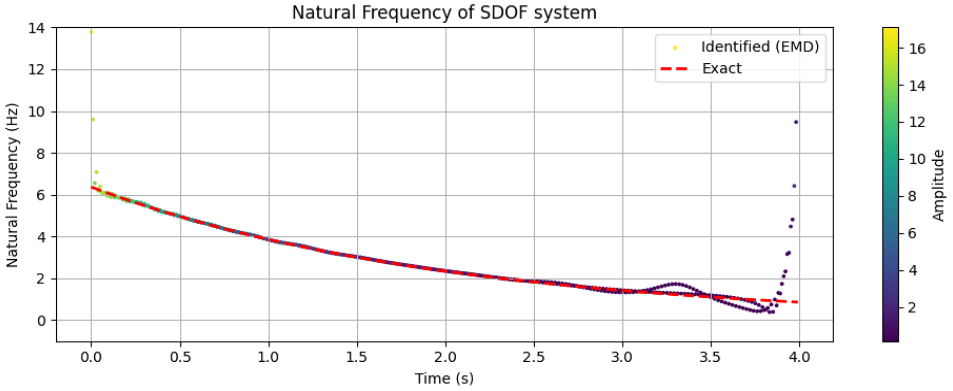

(a) EMD

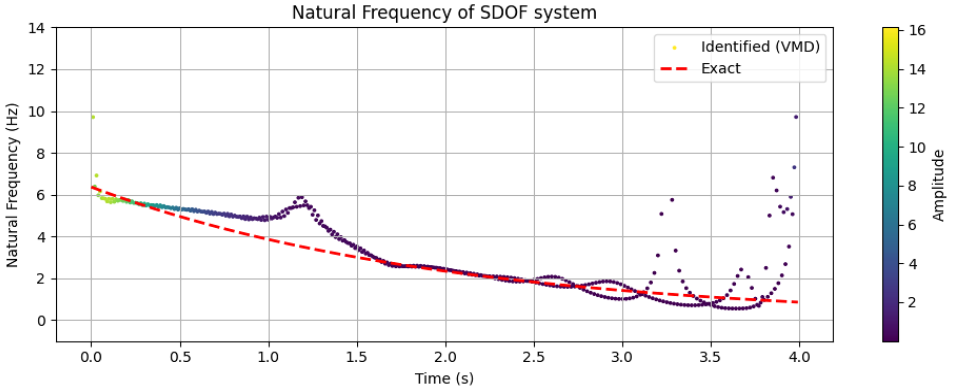

(b) VMD

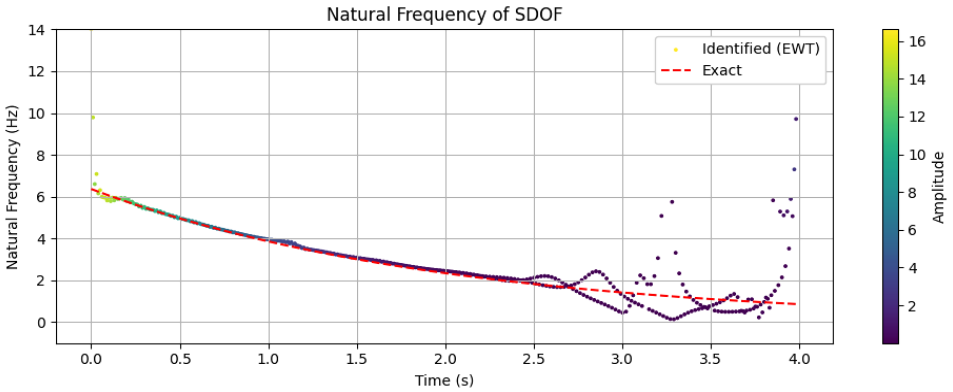

(c) EWT

Figure 9. Natural frequency of the SDOF system versus exact value

Overall, EMD provides the most accurate frequency identification, followed closely by EWT, while VMD exhibits slightly larger deviations. These results suggest that for single-dominant, smoothly varying systems, adaptive methods such as EMD offer superior tracking performance. However, instantaneous frequency estimation remains sensitive when structural responses become weak.

4. Experimental Investigation of the Discharging Silo and Signal Processing

4.1. Experimental Investigation of the Discharging Silo

Only a few studies have measured the dynamic response signals of a discharging silo. In this study, experimental data on the silo's dynamic response provided by Griffiths [14] are used for signal analysis. Griffiths [14] designed several experiments to reproduce the booming sound using a 2000 mm long polycarbonate hollow tube and investigated the relationships among amplitude, frequency, discharge rate, and moisture content. The internal diameter of the polycarbonate tube was 194 mm, and the wall thickness was 3 mm. The tube was supported by a steel frame with five interchangeable top plates. Each plate was drilled with a central hole serving as an outlet, allowing variation of the

discharge rate. The selected hole diameters were 60 mm, 90 mm, 120 mm, and 194 mm. To measure the dynamic response, eight accelerometers (model 393B04, manufactured by PCB) were attached to the exterior surface of the silo wall, as shown in Figure 10. These sensors were connected to a QuantumX MX840B data logger operating at a sampling rate of 1200 Hz. The PCB 393B04 accelerometers have a measurement range of ±5g and are capable of capturing frequencies between 0.06 Hz and 450 Hz. Sand was used as the discharging material in all experiments. Sand has been reported in the literature to reliably produce vibrations and booming sounds. A sieving procedure was followed to retain particle sizes between 300 – 600 µm.

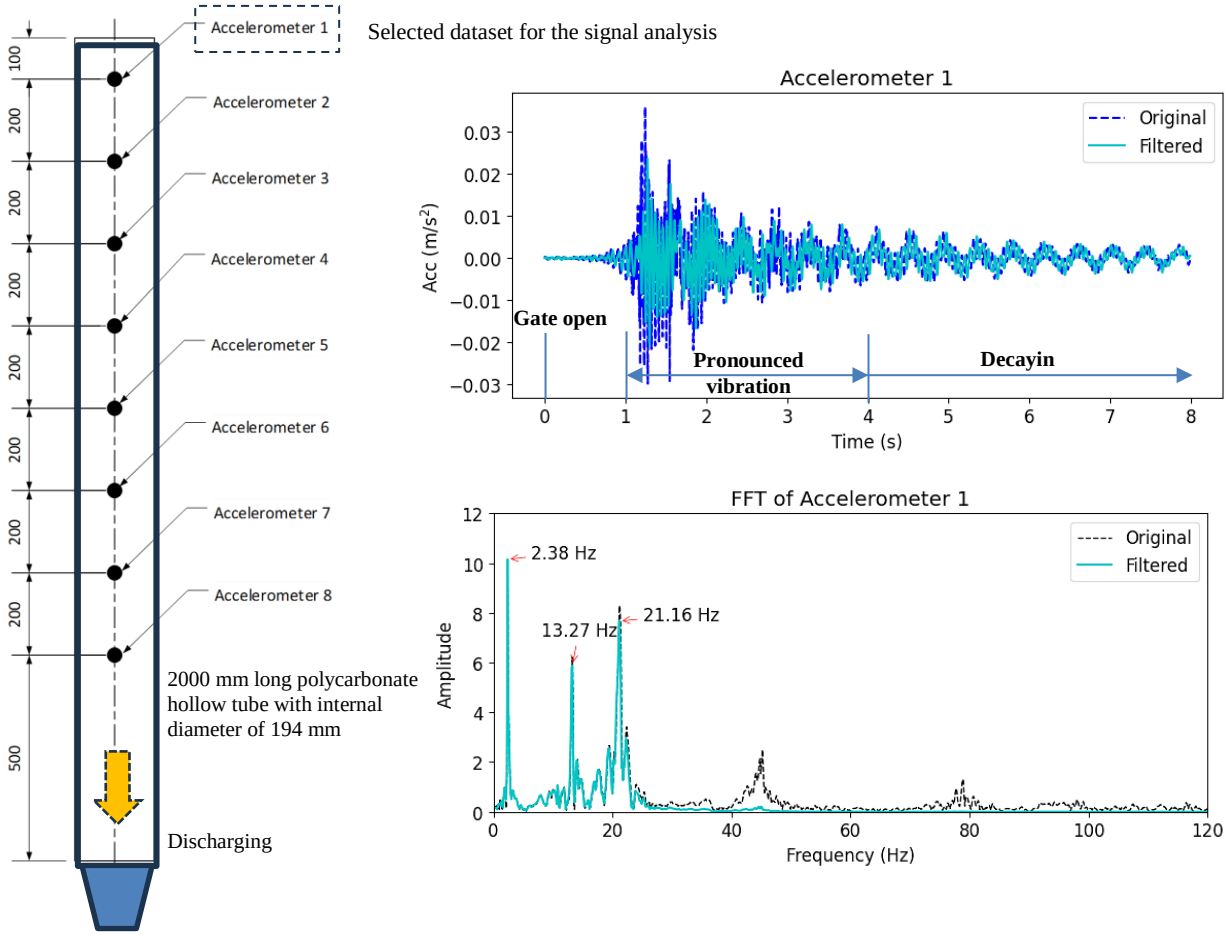

Figure 10. Locations of accelerometers mounted on the tube

For the purposes of this study, acceleration data collected from Accelerometer 1 (located at the topmost position) during discharge through a 150 mm outlet with a moisture content of 7.84% are analyzed. This dataset was selected because it represents a critical flow rate and produces a strong structural response. The measured acceleration data were denoised using the Daubechies wavelet (db10) with a decomposition level of 2. Universal thresholding was applied using a hard-threshold rule, and the noise variance was estimated in a level-dependent manner to improve denoising robustness while preserving structural dynamic characteristics. The acceleration time history from Accelerometer 1 and its corresponding Fourier spectrum, with marked dominant peaks, are shown in Figure 10.

4.2. Observation of the Signal

The denoised acceleration signal shown in Figure 10 indicates that the first two seconds of the discharge cycle produce relatively large accelerations compared to the later stages. As observed by Griffiths [14], a loud foghorn-like sound was heard during the first few seconds after the gate at the bottom of the tube was opened to allow the sand particles to flow out. The sound dissipated once approximately half of the sand volume had been discharged. Prior to discharge, the tube wall was elastically stretched radially and shortened longitudinally. When the gate was opened, the elastically deformed structure rebounded, compressing the column of sand particles inside. The reaction force from the sand column then acted on the tube wall. Pronounced wall accelerations, caused by the interaction between the elastically deformed wall and the sand particles, were observed. Similar phenomena were reported by Xu & Liang [11]. The accelerations observed during the final five seconds (3-8 s) appear more sinusoidal, containing multiple lower-frequency components with longer periods compared to the earlier phase, and gradually decay toward zero.

4.3. Signal Processing of the Mono-Component Signal

4.3.1. Empirical Mode Decomposition (EMD)

Figure 11-a shows the first six mono-component modes extracted using EMD, together with the corresponding correlation factors. The correlation coefficients confirm that Modes 1–3 contain most of the signal energy, whereas higher modes represent secondary or low-amplitude components. The decomposition results are explained as:

- Mode 1, with the highest correlation factor (r = 0.509), captures high-frequency oscillations at the beginning of the signal and becomes nearly flat after approximately 2 s. This behavior is consistent with the acceleration signal shown in Figure 10.
- Modes 2 to 4 progressively represent mid-frequency oscillations associated with the pronounced vibration stage.
- Modes 5 and 6 contain lower-frequency and slowly varying components corresponding to the decaying phase of the response.

These mono-component modes were analyzed using the Hilbert spectrum to illustrate instantaneous frequency. Figure 11-b shows the instantaneous frequency with a color bar indicating amplitude (energy content). Modes 1 and 2 show wide frequency dispersion, including negative frequencies. These negative values are not physically meaningful for structural vibration and indicate artifacts introduced by Hilbert Transform instability when applied to non-ideal mono-component signals or low-amplitude data. In contrast, Modes 3 and 4 exhibit clear and coherent time-frequency trends. The frequencies remain within a realistic and positive ranges: 0–30 Hz in Mode 3, 5-15 Hz in Mode 4, and 2-5 Hz in Mode 5. These bands align well with the FFT peaks in Figure 10, confirming that EMD effectively separates the dominant vibration components. However, frequency spreading and sign changes in the early modes indicate moderate mode-mixing effects and sensitivity of the Hilbert spectrum to noise.

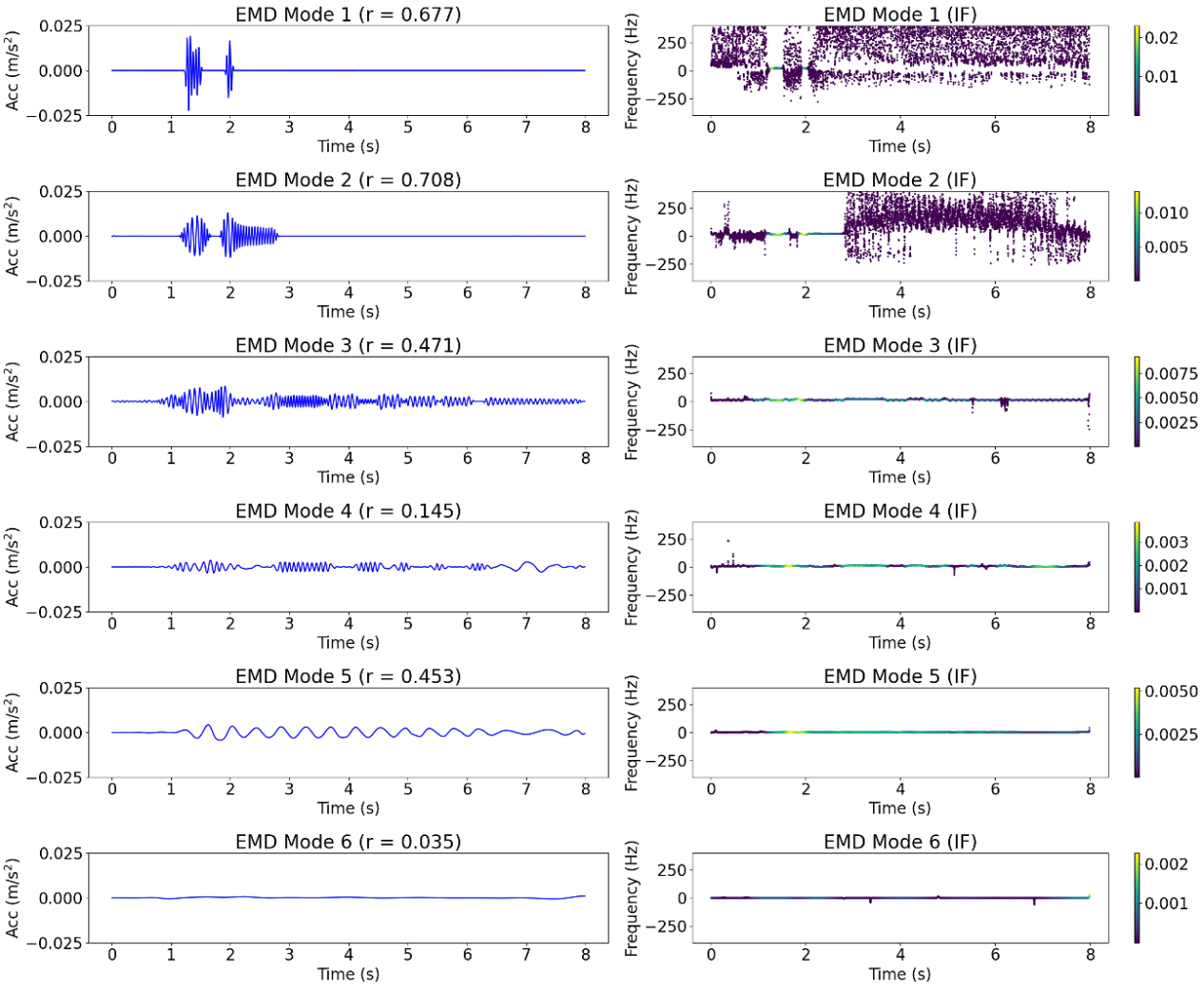

(a) EMD mono component (b) Instantaneous frequency

Figure 11. Silo signal processing using EMD

4.3.2. Variational Mode Decomposition (VMD)

Figure 12-a presents the six modes obtained using VMD. Unlike EMD, VMD exhibits narrowband oscillations, indicating effective decomposition into mono-components. Modes 3-6 show strong oscillatory behavior and relatively high correlation values (r = 0.47–0.76), suggesting that they capture most of the signal's energy. The waveform envelopes are smoother and more regular compared to those from EMD, reflecting VMD's optimization-based separation. The instantaneous frequencies of each mono-component mode, shown in Figure 12-b, are more concentrated than those obtained using EMD. However, small fluctuations are still observed, especially during the low-amplitude decay stage.

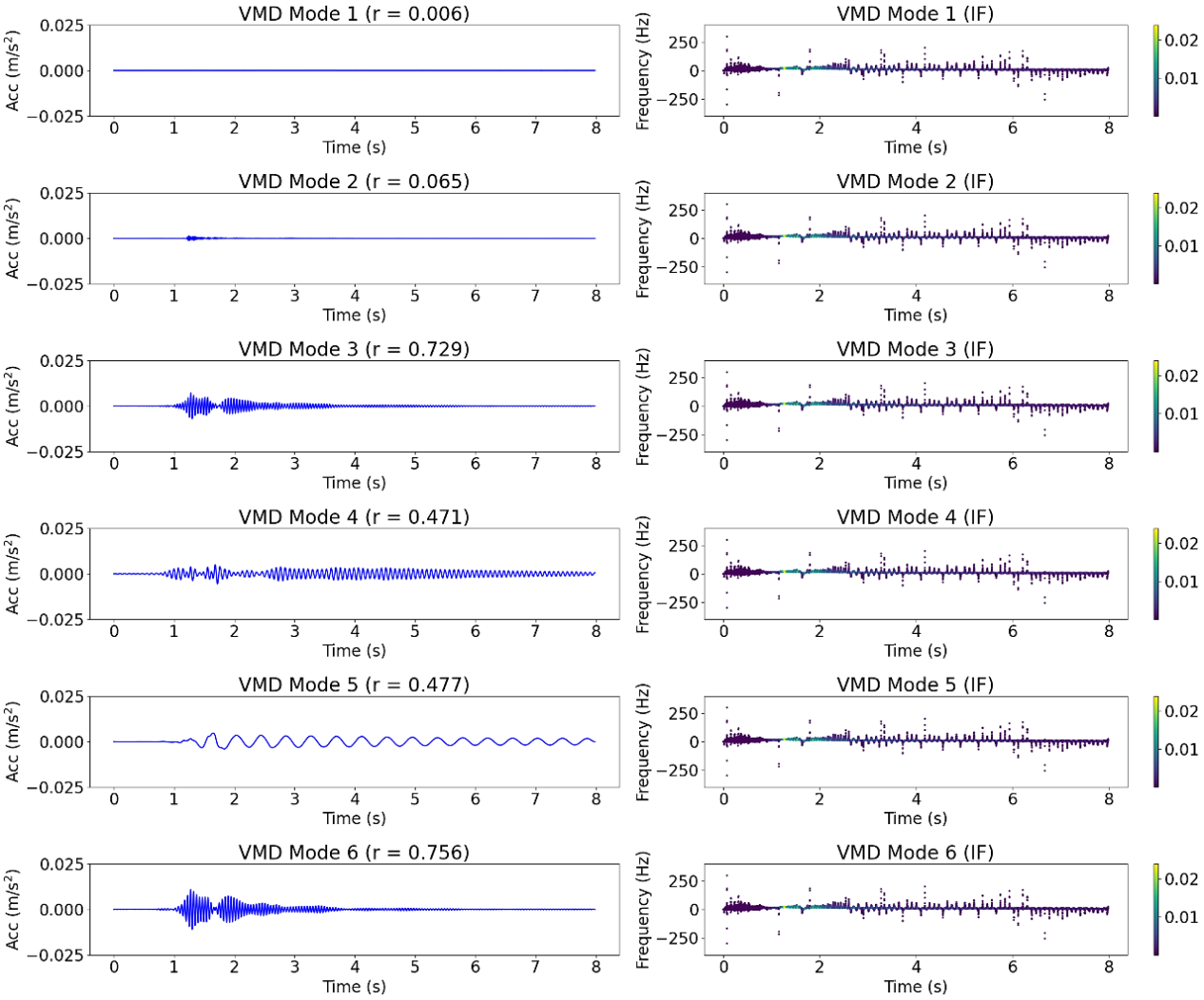

(a) VMD mono component (b) Instantaneous frequency

Figure 12. Silo signal processing using VMD

Overall, VMD achieves clearer spectral partitioning than EMD and reduces mode mixing. Nevertheless, minor frequency instability remains when the vibration amplitude diminishes.

4.3.3. Empirical Wavelet Transform (EWT)

Figure 13-a displays the EWT decomposition results. Because EWT performs adaptive segmentation in the frequency domain before reconstructing wavelet filters, the resulting modes reflect distinct spectral bands.

Modes 1 and 2 exhibit strong time-localized transients early in the signal (approximately 1–2.5 s), corresponding to the pronounced vibration stage observed in Figure 10. Their high correlation values (r = 0.677 and 0.708) indicate strong relevance to the original signal. However, Mode 1 contains significant noise, as observed in the Hilbert spectrum. Mode 3 represents mid-frequency oscillations, while Mode 5 captures the low-frequency trend corresponding to the 2–5 Hz band identified in the FFT. As shown in Figure 13-b, the instantaneous frequencies are generally stable and concentrated within physically meaningful positive ranges. Similar to EMD and VMD, some deviation occurs during the late decay stage due to amplitude reduction and increased sensitivity of phase differentiation.

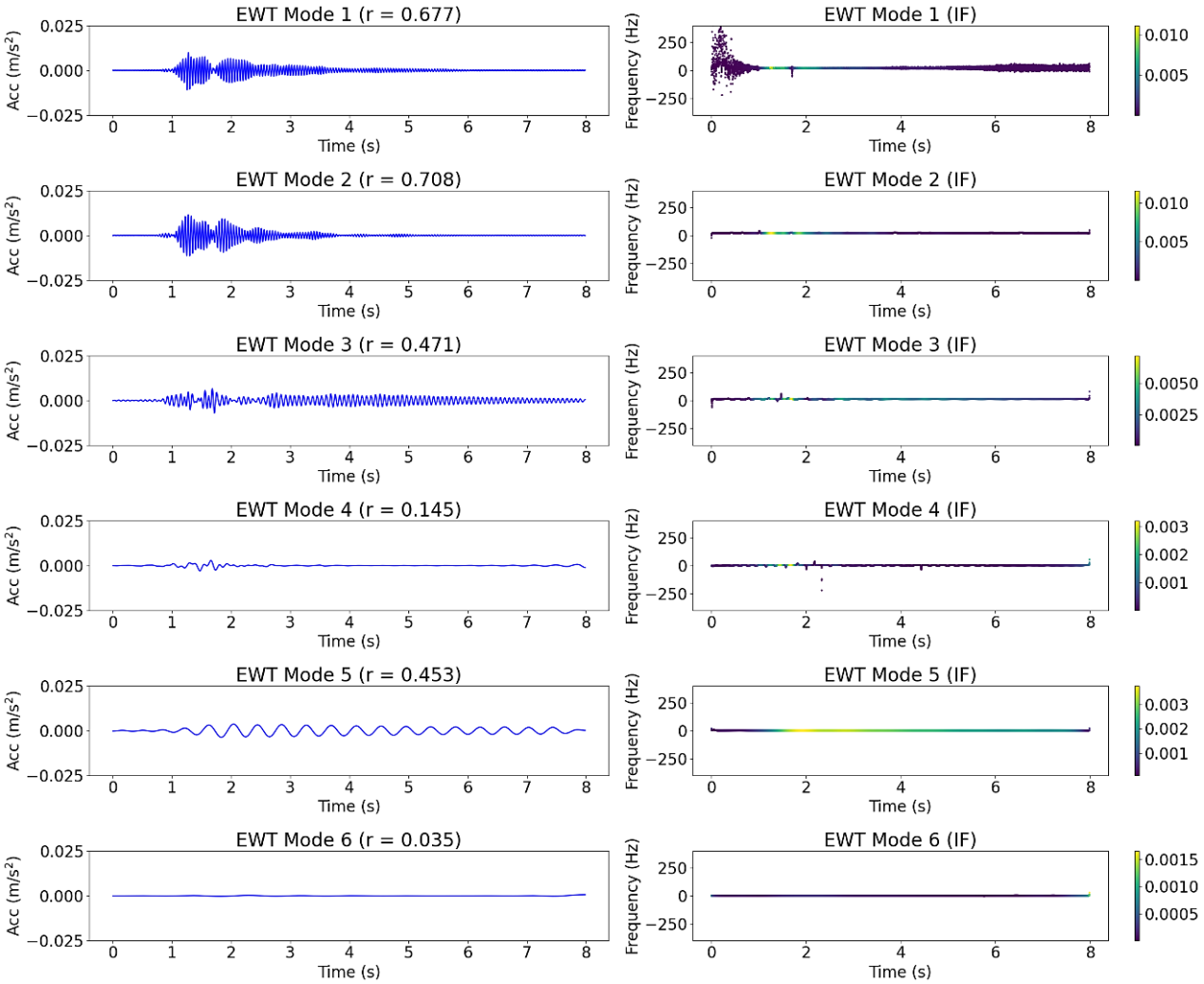

(a) EWT mono component (b) Instantaneous frequency

Figure 13. Silo signal processing using EWT

4.4. Weighted-average Instantaneous Frequency

To filter out negative and erratic frequencies, a weighted combination of the mono-component modes was applied, as described in Equation 7. The resulting weighted-average instantaneous frequency is shown in Figure 14. As seen in Figure 11-b, Modes 1 and 2 are scattered and noisy, therefore, the weighted combination considers Modes 4 to 6 for EMD. Similarly, Modes 1 and 2 are excluded from the VMD calculation due to their very small correlations (Figure 12-a). For EWT, Mode 1 is excluded due to the observed noise in Figure 13-b. From Figures 14, for all methods, the high-energy frequency content is primarily concentrated between 8–20 Hz during the 1-2 second interval. The amplitude is clearly represented using a color bar (with yellow indicating high amplitude), corresponding to the major excitation observed in the experiment [14]. The dominant frequency gradually drifts downward over time, which is consistent with a decaying oscillatory source.

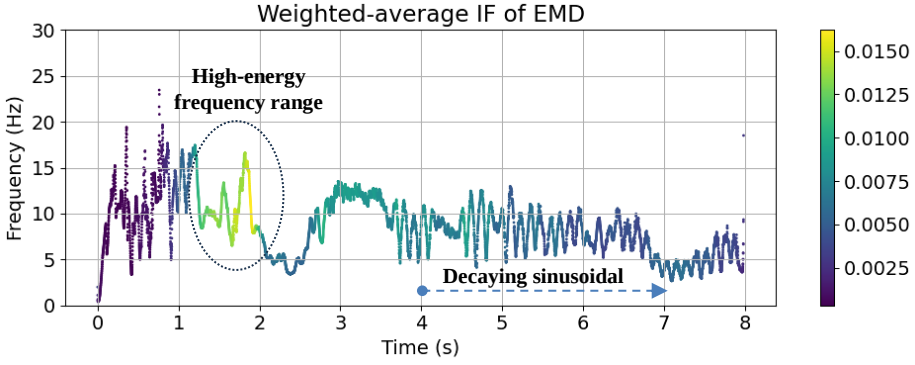

(a) EMD weighted-average instantaneous frequency (Excluding Modes1 and 2)

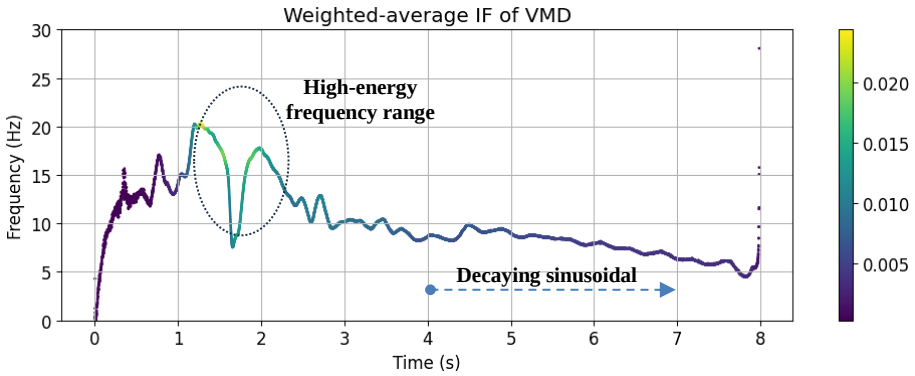

(b) VMD weighted-average instantaneous frequency (Excluding Modes1 and 2)

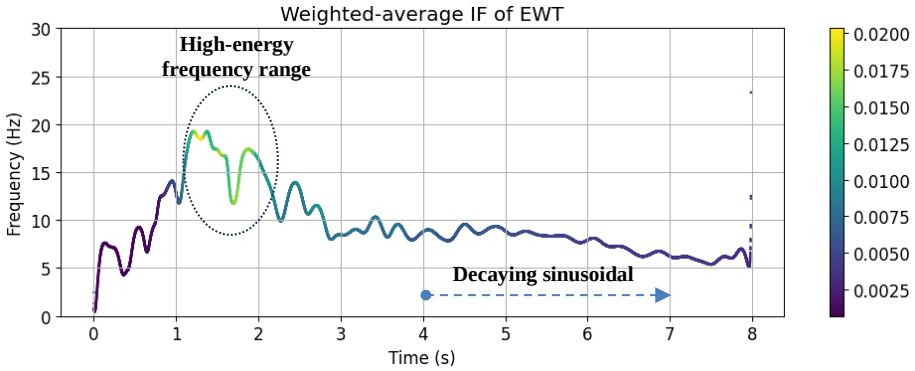

(c) EWT weighted-average instantaneous frequency (Excluding Modes1)

Figure 14. Weighted-average instantaneous frequency

4.5. Frequency Domain Analysis

Frequency domain analysis provides the dominant frequencies of a signal, offering an overview of its vibration content; however, it does not capture instantaneous frequency variations. In this study, the denoised signal was analyzed in the frequency domain using the same three signal processing methods previously applied for instantaneous frequency analysis: EMD, EWT, and VMD. The results are shown in Figure 15. In addition, the conventional Fourier Transform (FT) is also presented. Figure 15 shows that the four signal processing methods yield slightly different results. However, when focusing on the 4-8 s interval, the dominant frequencies identified by each method appear similar, as illustrated in Figure 16. This consistency is attributed to the nature of the raw signal during the final four seconds of the discharge cycle, which is predominantly sinusoidal and decays slowly.

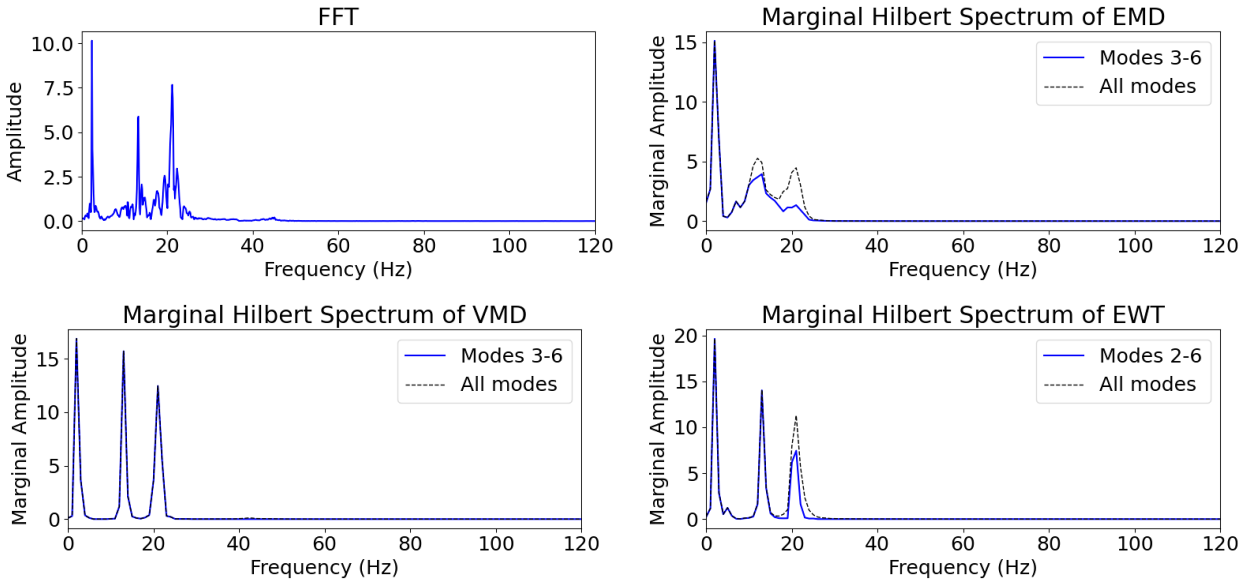

Figure 15. Frequencies for the entire duration of the discharge cycle

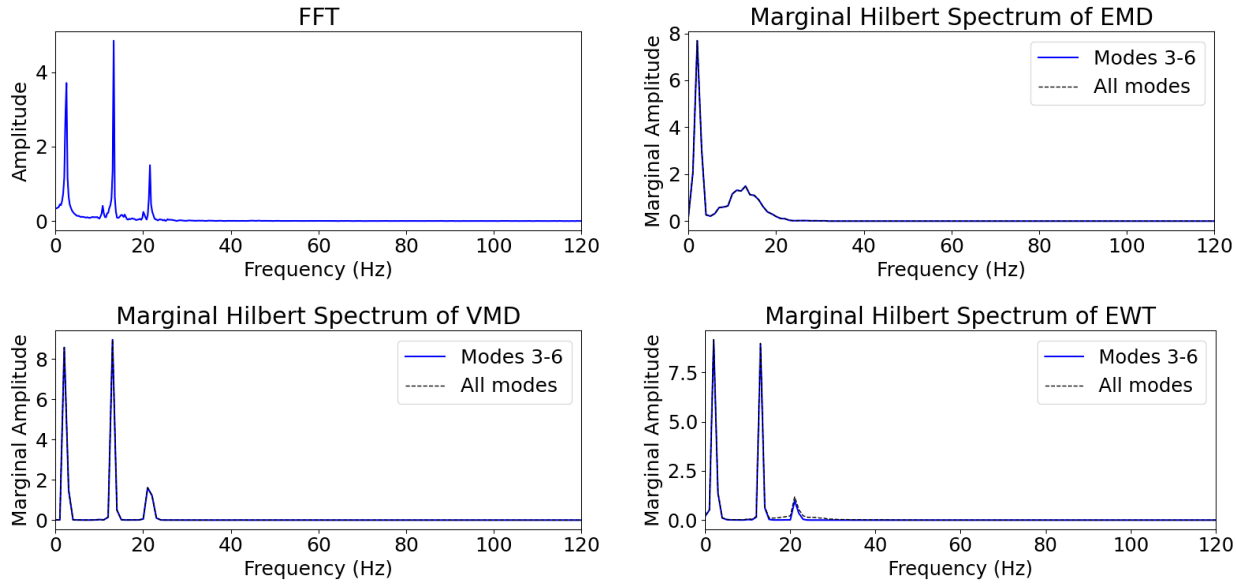

Figure 16. Frequencies during the last four seconds of the discharge cycle

5. Conclusion

This study systematically evaluated the capabilities of three advanced signal decomposition techniques—Empirical Mode Decomposition (EMD), Variational Mode Decomposition (VMD), and Empirical Wavelet Transform (EWT)—for instantaneous frequency identification in time-varying mass (TVM) engineering structures.

Validation was first conducted using an artificial nonlinear signal and a time-varying parameter SDOF system with known frequency evolution. In these controlled numerical cases, all three methods successfully captured the time-dependent frequency variation. However, EMD provided the closest agreement with the exact analytical frequency history. Its fully adaptive nature allowed accurate tracking when the signal was clean and well-defined. In contrast, VMD and EWT showed minor deviations due to bandwidth constraints and predefined spectral segmentation, respectively, although their overall performance remained acceptable.

When applied to experimental silo discharge data, the signal characteristics became significantly more complex due to noise, transient bursts, and multi-frequency interactions between the granular material and the container wall. Under these realistic conditions, VMD and EWT demonstrated more stable and physically interpretable decompositions, whereas EMD exhibited greater sensitivity to noise and mode mixing.

The implementation of a weighted-average instantaneous frequency approach effectively reduced spurious and negative frequency artifacts, enabling clearer identification of dominant frequency bands. The results confirm that no single technique is universally superior; rather, method selection should depend on signal quality and application context. For controlled simulations, EMD is highly effective, whereas VMD and EWT are preferable for noisy field measurements. Overall, the findings highlight the importance of integrating instantaneous frequency analysis into the dynamic assessment and design framework of TVM structures, particularly for improving structural reliability and monitoring strategies.

6. Declarations

6.1. Author Contributions

Conceptualization, C.B., C.H., V.V., and P.T.; methodology, C.B., C.H., and P.T.; formal analysis, C.B. and P.T.; investigation, C.B., C.H., and P.T.; data curation, C.B. and P.T.; writing—original draft preparation, C.B.; writing—review and editing, C.H., T.S., V.V., P.T., W.S., S.L., and P.C.; visualization, C.B.; supervision, C.H., T.S., V.V., W.S., S.L., and P.C. All authors have read and agreed to the published version of the manuscript.

6.2. Data Availability Statement

The data presented in this study are available on request from the corresponding author.

6.3. Funding

This research would not have been possible without the invaluable support and contributions of several individuals and institutions. This project was funded by National Research Council of Thailand (NRCT) and Chiang Mai University under project codes N42A670307 and 2025 Fundamental Fund.

6.4. Conflicts of Interest

The authors declare no conflict of interest.

7. References

[1] Kanthakasikam, R., Charatpangoon, B., Hansapinyo, C., Buachart, C., & Kiyono, J. (2024). Seismic Safety Analysis of Dam Appurtenant Structures in Northern Thailand. KSCE Journal of Civil Engineering, 28(7), 2885–2896. doi:10.1007/s12205-024-1421-9.

[2] Ketiyot, R., & Hansapinyo, C. (2018). Seismic performance of interior precast concrete beam-column connections with t-section steel inserts under cyclic loading. Earthquake Engineering and Engineering Vibration, 17(2), 355–369. doi:10.1007/s11803-018-0446-9.

[3] Deng, Y., Guo, Z., Zhang, H., Limkatanyu, S., Sukontasukkul, P., Yuen, T. Y. P., Wong, S. H. F., Hansapinyo, C., Adom-Asamoah, M., Shen, M., Huang, L., Kuang, J. S., & Zou, Y. (2023). Experimental study on flexural behaviours of fresh or aged hollow reinforced concrete girders strengthened by prestressed CFRP plates. Engineering Structures, 294, 116776. doi:10.1016/j.engstruct.2023.116776.

[4] Buachart, C., Hansapinyo, C., Tantisukhuman, N., Miyamoto, M., Matsushima, M., Limkatanyu, S., Imjai, T., & Zhang, H. (2023). Real time vibration measurement and inverse analysis for dynamic properties of an axisymmetric masonry structure. Journal of Asian Architecture and Building Engineering, 22(4), 2237–2246. doi:10.1080/13467581.2022.2145212.

[5] Hansapinyo, C., Vimonsatit, V., Matsushima, M., & Limkatanyu, S. (2021). Critical amount of corrosion and failure behavior of flexural reinforced concrete beams. Construction and Building Materials, 270, 121448. doi:10.1016/j.conbuildmat.2020.121448.

[6] Tu, P., & Vimonsatit, V. (2017). Silo quaking of iron ore train load out bin – A time-varying mass structural dynamic problem. Advanced Powder Technology, 28(11), 3014–3025. doi:10.1016/j.apt.2017.09.012.

[7] BS EN 1991-4:2006 (2006). Eurocode 1: Actions on structures - Part 4: Silos and tanks. European Committee for Standardization, Brussels, Belgium.

[8] AS 3774-96. (1996). Loads on bulk solids containers. Australian Standard, Sydney, Australia.

[9] ACI 313-16. (2016). Design Specification for Concrete Silos and Stacking Tubes for Storing Granular Materials. American Concrete Institute (ACI), Michigan, United States.

[10] Tu, P., & Vimonsatit, V. (2021). Concrete silos: Failures, design issues and repair/ strengthening methods. Applied Sciences (Switzerland), 11(12), 3938. doi:10.3390/app11125675.

[11] Xu, Z., & Liang, P. (2022). Modified lateral pressure formula of shallow and circular silo considering the elasticities of silo wall and storage materials. Scientific Reports, 12(1), 7069. doi:10.1038/s41598-022-11305-6.

[12] Rotter, J. M. (2009). Silo and Hopper Design for Strength. Bulk Solids Handling: Equipment Selection and Operation. Blackwell Publishing, Oxford, United Kingdom. doi:10.1002/9781444305449.ch3.

[13] Tu, P., Vimonsatit, V., & Hansapinyo, C. (2023). The Influence of Moisture on the Frequency Spectrum of Time Varying Mass Engineering Structure. Civil Engineering Journal (Iran), 9(1), 17–28. doi:10.28991/CEJ-2023-09-01-02.

[14] Griffiths, J. (2018). Impact of moisture content on the dynamic response of a Silo Model Wall during discharge. Curtin University, Perth, Australia.

[15] de Medeiros, A. S., & da Silva, M. A. V. (2025). Influence of Emulsion Type and Moisture on the Stiffness of Stabilized Granular Soil. Civil Engineering Journal, 11(6), 2282–2302. doi:10.28991/CEJ-2025-011-06-07.

[16] Kebeli, H. V., Bucklin, R. A., Ellifritt, D. S., & Chau, K. V. (2000). Moisture-induced pressures and loads in grain bins. Transactions of the American Society of Agricultural Engineers, 43(5), 1211–1221. doi:10.13031/2013.3014.

[17] Chen, Y., Liang, C., Wang, X., Guo, X., Chen, X., & Liu, D. (2020). Static pressure distribution characteristics of powders stored in silos. Chemical Engineering Research and Design, 154, 1–10. doi:10.1016/j.cherd.2019.10.050.

[18] Sadowski, A. J., & Rotter, J. M. (2011). Buckling of very slender metal silos under eccentric discharge. Engineering Structures, 33(4), 1187–1194. doi:10.1016/j.engstruct.2010.12.040.

[19] Xin, Y., Hao, H., & Li, J. (2019). Time-varying system identification by enhanced Empirical Wavelet Transform based on Synchroextracting Transform. Engineering Structures, 196. doi:10.1016/j.engstruct.2019.109313.

[20] Ma, C. C., Zhang, X. N., Dai, X. J., Zhou, C. C., & Guo, Z. H. (2019). Transverse vibration control of an axially moving beam system with time varying mass. Zhendong Gongcheng Xuebao/Journal of Vibration Engineering, 32(3), 396–403. doi:10.16385/j.cnki.issn.1004-4523.2019.03.003.

[21] Tu, P., Vimonsatit, V., & Hansapinyo, C. (2022). Frequency spectrum of engineering structures with time varying masses. Journal of Infrastructure Preservation and Resilience, 3(1), 15. doi:10.1186/s43065-022-00059-0.

[22] Hernández-Juárez, J. R., López-Villa, A., Medina, A., & Serrano Huerta, D. A. (2025). Low-Frequency Acoustic Emissions During Granular Discharge in Inclined Silos. Fluids, 10(5), 138. doi:10.3390/fluids10050138.

[23] Shang, X. Q., Huang, T. L., He, Y. Bin, & Chen, H. P. (2024). Operational Modal Analysis of Civil Engineering Structures with Closely Spaced Modes Based on Improved Hilbert–Huang Transform. Sensors, 24(23), 7600. doi:10.3390/s24237600.

[24] Huang, N. E., Shen, Z., Long, S. R., Wu, M. C., Snin, H. H., Zheng, Q., Yen, N. C., Tung, C. C., & Liu, H. H. (1998). The empirical mode decomposition and the Hubert spectrum for nonlinear and non-stationary time series analysis. Proceedings of the Royal Society A: Mathematical, Physical and Engineering Sciences, 454(1971), 903–995. doi:10.1098/rspa.1998.0193.

[25] Dragomiretskiy, K., & Zosso, D. (2014). Variational mode decomposition. IEEE Transactions on Signal Processing, 62(3), 531–544. doi:10.1109/TSP.2013.2288675.

[26] Gilles, J. (2013). Empirical wavelet transform. IEEE Transactions on Signal Processing, 61(16), 3999–4010. doi:10.1109/TSP.2013.2265222.

[27] Kaslovsky, D. N., & Meyer, F. G. (2010). Noise corruption of Empirical Mode Decomposition and its effect on instantaneous frequency. Advances in Adaptive Data Analysis, 2(3), 373–396. doi:10.1142/S1793536910000537.

[28] Wardana, A. N. I. (2017). A comparative study of EMD, EWT and VMD for detecting the oscillation in control loop. In Proceedings - 2016 International Seminar on Application of Technology for Information and Communication, ISEMANTIC 2016, 58–63. doi:10.1109/ISEMANTIC.2016.7873810.

[29] Chen, J., & Zhao, G. (2014). Numerical and experimental investigation on parameter identification of time-varying dynamical system using hilbert transform and empirical mode decomposition. Mathematical Problems in Engineering, 2014(1), 568637. doi:10.1155/2014/568637.

[30] Wang, Z. C., Ren, W. X., & Chen, G. (2018). Time–frequency analysis and applications in time-varying/nonlinear structural systems: A state-of-the-art review. Advances in Structural Engineering, 21(10), 1562–1584. doi:10.1177/1369433217751969.

[31] Li, Q. S., Fang, J. Q., & Liu, D. K. (2000). Exact solutions for free vibration of single-degree-of-freedom systems with nonperiodically varying parameters. JVC/Journal of Vibration and Control, 6(3), 449–462. doi:10.1177/107754630000600307.